Tanabe, Minoru; Shitomi, Hiroshi; Dönsberg, Timo; Ikonen, Erkki

Characterization of predictable quantum efficient detector in terms of optical non-linearity in the visible to near-infrared range

Published in:
Metrologia

DOI:
10.1088/1681-7575/ac1e35

Published: 01/10/2021

Document Version
Peer reviewed version

Please cite the original version:
Tanabe, M., Shitomi, H., Dönsberg, T., & Ikonen, E. (2021). Characterization of predictable quantum efficient detector in terms of optical non-linearity in the visible to near-infrared range. *Metrologia*, *58*(5), [055012]. https://doi.org/10.1088/1681-7575/ac1e35

Characterization of predictable quantum efficient detector in terms of optical nonlinearity in the visible to near-infrared range

Minoru Tanabe[1], **Hiroshi Shitomi**[1], **Timo Dönsberg**[2]‡, **and Erkki Ikonen**[2,3]

[1] National Metrology Institute of Japan, National Institute of Advanced Industrial Science and Technology, 1-1-1 Umezono, Tsukuba, Ibaraki, Japan

[2] VTT Technical Research Centre of Finland Ltd, Espoo, Finland

[3] Metrology Research Institute, Aalto University, Espoo, Finland

E-mail: tanabe-m@aist.go.jp

Abstract. Characteristics of predictable quantum efficient detector (PQED) by in terms of optical nonlinearity in the visible to near-infrared range were investigated under zero-bias and reverse-bias voltage conditions. In the zero-bias condition, linear behavior was observed in the wavelength from 405 nm to 1060 nm in the photocurrent range of 1 nA to 10 μA, and saturation occurred for photocurrents over 10 μA for all wavelengths. In the reverse-bias voltage of 10 V, the linear behavior was observed in the photocurrent range of 64 nA to 1 mA except for the wavelength of 1060 nm, and the saturation photocurrent increased up to 1 mA. Supralinearity value at 1060 nm sharply increased from the photocurrent of 100 μA, and its maximum value reached up to 0.34 % at the photocurrent of 1 mA because of the back surface recombination and the longer absorption length. The spectral linearity results of the PQED help us to understand the charge-carrier loss mechanism in the PQED, and would lead to more accurate optical measurement with it.

Keywords: Radiometry, Photometry, Silicon photodiode, Linearity

1. Introduction

An accurate absolute radiant flux scale is required in the fields of radiometry and photometry. The realization of the scale can be done using primary optical detectors. These detectors are separated into two types: thermal detector and quantum detector, according to the principle of light detection. Thermal detectors used as primary standards at cryogenic temperatures can reach low uncertainties [1, 2]. Values down to about 0.01 % are achieved in the measurement uncertainty of the absolute radiant flux in the visible to near-infrared wavelength region. However, the cryogenic radiometer

‡ Present address: National Institute of Standards and Technology, Boulder, CO, USA.

needs to be kept at the temperature around 10 K during its operation, and a range of dynamic optical flux levels is limited to less than a few orders of magnitude.

Quantum detectors, such as silicon (Si) photodiodes (PDs) and photomultiplier tubes, convert the incident photon flux to charge carriers. Si PDs have several advantages, including their low dark current, wide wavelength range, and fast response. The possibility of using commercial Si PDs as primary standards of optical flux has been examined since the early-1980s [3, 4, 5, 6]. However, the true capability of these quantum detectors as a primary standard is still one of the research topics [7, 8]. Using specially-designed induced junction PDs, predictable quantum efficient detector (PQED) was developed and its feasibility as a primary standard was demonstrated in [9, 10, 11, 12, 13]. The PQED is constructed with two Si PDs configured into a light-trapping structure [14, 15]. In an ideal quantum detector, conversion ratio of incident photons into generated electron-hole pairs is unity. However, quantum detectors have two loss mechanisms in this conversion process; the reflectance of the detector and the internal quantum deficiency. The concept of the PQED is to reduce the losses, so that their values can be predicted with small enough uncertainty. The total uncertainty level of 0.01 % for the absolute radiant flux is obtained at room temperature. The advantage of the PQED is that it can be operated at room temperature, can be portable, and it is easy to use as compared to cryogenic radiometer. The PQED has been utilized for high-accuracy optical measurements in visible region, including a new realization of the photometric scale [16, 17, 18].

Another advantage of using the quantum detector such as Si PDs in determining the absolute radiant flux is that it helps us to extend measurable flux range much larger than six orders of magnitude. The measured photocurrent for the PQED was tens of nano-amperes in the optical measurement with light-emitted-diodes [17], miliamperes in the absolute radiant flux measurement with stabilized lasers [12], and pW levels in the absolute radiant flux measurement with a stabilized laser at a cryogenic temperature [19]. Thus, the linearity of Si PD with respect to the incident radiant flux at various wavelengths is a fundamental element to determine the absolute radiant flux in a range greater than six orders of magnitude, because it would show nonlinear response at a certain radiant flux level with a decrease or increase in responsivity [20, 21, 22]. The decrease in the responsivity is saturation, which is caused by PD series resistance under zero-bias condition. The increase in the responsivity is known as supralinearity, which is caused by the recombination losses of the generated minority carriers in the Si bulk and on the PD surface. The nonlinearity of the PD can be defined as a combination of two nonlinear phenomena: saturation and supralinearity, which occur in the high radiant flux level. Several studies have been performed to evaluate the nonlinearity of the PQED [10, 12, 23]. These results concluded that the PQEDs show the linear response at the wavelengths of 488 nm and 760 nm in the optical flux range of seven orders of magnitude. In these studies, the appropriate reverse bias voltages also applied to them. However, these studies focused on the nonlinearity evaluation in the limited wavelength range, which would be insufficient to discuss full characterization of the spectral nonlinearity of the PQED for the purpose of modelling the charge-carrier losses in the PDs [24]. Therefore, more accurate and detailed linearity measurement of the PQED for various wavelengths under zero-bias and reverse-bias voltage conditions is required to make the best use of the PQED in the fields of radiometry and photometry. Two types of the nonlinearity values, supralinear behavior, and their starting photocurrents in the visible to near-infrared range also should be qualitatively evaluated to characterize the performance of the PQED.

In this study, we report on the spectral linearity of the PQED based on n-type Si PDs [12] in the visible to near-infrared region under zero-bias and reverse-bias voltage conditions. For the first time, we show linear response of the PQED in visible to near-infrared region with the reverse-bias voltage of 10 V. The upper limit of the spectral linearity range is found at 1060 nm, where the PQED shows supralinear behaviour.

2. Experimental setup

2.1. Predictable quantum efficient detector

A PQED based on n-type Si PDs was used for evaluating the spectral linearity. The PDs were manufactured by VTT Technical Research Centre of Finland [12]. The PQED is constructed using two induced junction PDs, configured into a light-trapping structure. To suppress the recombination losses in the Si bulk and the surface of Si PD, the PDs are made of a high-purity Si substrate, coated by an aluminum oxide (Al_2O_3) layer. By applying an appropriate reverse bias voltage, the depletion layer extends to a depth of tens of micrometers into the Si bulk and increases the collection efficiency of the generated charge carriers. The spectral internal quantum deficiency and reflectance loss of the used Si PD were evaluated in advance. The PD thickness was 500 μm. Further details of the PQED prameters are given in [12]. Nitrogen flow system is available to protect the n-type Si PDs from dust, where nitrogen of impurity concentration less than 1 ppm was fed into the PQED. Its flow rate was adjusted to be 1.5 L/min.

2.2. Spectral linearity evaluation

The spectral linearity measurements of the PQED were performed with the flux addition method [21, 22], as shown in Fig. 1. In this setup, seven Fabry-Perot laser diodes (FPLDs), a diode-pumped solid-state laser (DPSS), and an external cavity laser diode (ECLD) [25, 26] were used. Incident laser wavelengths were selected to be 405 nm 460 nm, 660 nm, 850 nm, 915 nm, 980 nm, and 1060 nm for the FPLDs, 530 nm for the DPSS, and 760 nm for the ECLD. All laser intensity drifts of approximately 0.03 % and wavelength drifts less than 0.01 % were attained by stabilization with Peltier coolers with temperature stability better than 0.01 °C. These lasers were operated with constant current source at room temperature of (23 ± 1) °C. Each beam was adjusted with a collimating lens and a convex lens, allowing us to create a near-Gaussian shape of 1.0 mm in $1/e^2$ diameter on PQED surface.

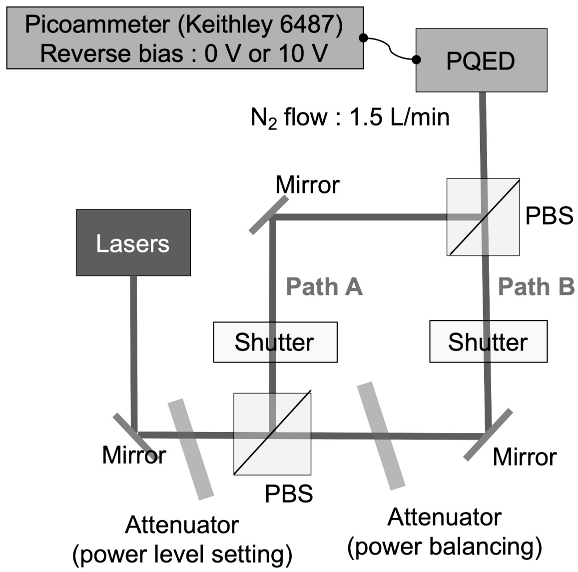

Figure 1. Schematic diagram of spectral linearity measurement for PQED.

The procedure of linearity measurement with the flux addition method is as following. The laser beam was divided into two paths (Path A and Path B) by applying a polarization beam-splitting (PBS) cube, shown in Fig. 1. The laser powers of two passes were adjusted to be identical using an optical attenuator. The both laser beams were aligned to the same spot on the PQED surface by adjusting two plane mirrors and another PBS cube. The beam position between the two spots was checked with a complementary metal-oxide-semiconductor image sensor before linearity measurements. By blocking one of the laser beams at a time and superimposing them on the PQED using two mechanical shutters, the generated photocurrents I_{A}, $I_{\mathrm{A+B}}$, I_{B}, $I'_{\mathrm{A+B}}$, and I'_{A} ($I_{\mathrm{A}} \simeq I'_{\mathrm{A}}$, $I_{\mathrm{A+B}} \simeq I'_{\mathrm{A+B}}$) were sequentially measured using a picoammeter (Keithley 6487). The photocurrents I_{A}, I_{B}, and $I_{\mathrm{A+B}}$ denote laser beam going through path A, path B, and both paths, respectively. An apostrophe indicates a repeated measurement. The difference between initial and repeated measurements is due to drift of laser power PQED response during the period of sequential measurements. The measurement range of the used picoammeter was kept the same during the flux addition process. The integration time of the picoammeter was adjusted to be 20 ms. The obtained spectral linearity of the PQED is determined by the performance of the first photodiode, where the incident radiation is mostly absorbed. The picoammeter was also used as a source to supply the reverse bias voltage to the PQED, which is applied with 10 V or is zero-bias condition. The bias voltage value of 10 V was selected to compare with the previous nonlinearity result [12]. The linearity factor $F_{\mathrm{LF}}(k)$ was obtained by averaging $F_{\mathrm{LF1}}(k)$ and $F_{\mathrm{LF2}}(k)$ as follows:

$$F_{\mathrm{LF1}}(k) = \frac{I_{\mathrm{A+B}}}{I_{\mathrm{A}} + I_{\mathrm{B}}}, \tag{1}$$

$$F_{\mathrm{LF2}}(k) = \frac{I'_{\mathrm{A+B}}}{I'_{\mathrm{A}} + I_{\mathrm{B}}}, \tag{2}$$

$$F_{\mathrm{LF}}(k) = \frac{F_{\mathrm{LF1}}(k) + F_{\mathrm{LF2}}(k)}{2}. \tag{3}$$

Three optical attenuators, two continuously variable neutral density filters and a step-variable neutral density filter, were used to adjust the photocurrent of 1 nA to tens mA. All attenuators were slightly tilted from the optical path to avoid the interference effect during the linearity measurements. By increasing the measured photocurrent by two times step, the nonlinearity factor, $F_{\mathrm{NL}}(n)$, of the PQED was obtained by multiplying successive linearity factors as follows:

$$F_{\mathrm{NL}}(1) = F_{\mathrm{LF}}(1) \quad (k = 1),$$

$$F_{\mathrm{NL}}(2) = F_{\mathrm{LF}}(1) \times F_{\mathrm{LF}}(2) \quad (k = 2),$$

$$\vdots$$

$$F_{\mathrm{NL}}(n) = F_{\mathrm{LF}}(1) \times F_{\mathrm{LF}}(2) \times \cdots \times F_{\mathrm{LF}}(n) \quad (k = n),$$

$$F_{\mathrm{NL}}(n) = \prod_{k=1}^{n} F_{\mathrm{LF}}(k). \tag{4}$$

Finally, the nonlinearity, $N(n)$, was derived with the obtained nonlinearity factor, $F_{\mathrm{NL}}(n)$, as follows:

$$N(n) = [F_{\mathrm{NL}}(n) - 1] \times 100. \tag{5}$$

All optical components and lasers in this system were kept in a dark box to maintain stable temperature of (23 ± 1) °C and no air stream. The PQED was kept in another dark box to suppress ambient light and stray light.

3. Results and discussion

3.1. Spectral linearity characteristics under zero-bias condition

Figure 2 shows the experimentally measured nonlinearity results at the wavelengths—405 nm 460 nm, 530 nm, 660 nm, 760 nm 850 nm, 915 nm, 980 nm, 1060 nm—for PQED under zero-bias condition. The solid horizontal lines in Fig. 2 represent the linear response. Assuming that the linearity factor, $F_{\mathrm{LF}}(0)$, at a generated photocurrent of 1 nA was equal to unity, the nonlinearities for each photocurrent were derived with Eqs. (4) and (5). The error bars shown on the plot represent the values obtained by calculating nonlinearity factors after obtaining linearity factors, which are based on the standard deviations of eight linearity factor measurements. The range discontinuities of the picoammeter are within these standard deviations. The range discontinuities are caused by the discontinuities of the A/D conversion in its internal electrical circuit.

As shown in Fig. 2, the values of the derived nonlinearity of the PQED were less than 0.1 % at the photocurrent from 1 nA to 10 μA in the selected wavelengths under the zero-bias condition. The responsivities started to decrease at the photocurrent over 10 μA in all wavelengths, which correspond to the saturation of the PQED. For the first time, it was experimentally shown that the PQED had linear response at least in the photocurrent level of 1 nA to 10 μA and such linear properties were hold in the wide wavelength range from the visible to near-infrared. It was also found that the PQED showed saturation around the photocurrent level of 10 μA under the zero-bias condition. This spectral linearity result is similar to the result for the PQED based on p-type Si PDs at 760 nm [23]. For other n-type Si PDs, the spectral supralinearity due to Shockley-Read Hall recombination loss [27, 28] and surface recombination loss [29] in the visible to near-infrared range have been reported [21, 22]. In contrast, the PQED response is expected to be linear because the recombination lifetime of the PQED is as long as 28 ms [12] and the recombination of the n-type Si with the Al_2O_3 coating makes the collection efficiency at the PD surface close to 100 %. This comparison infers that the PQED should not have any observable supralinearity at visible wavelengths, because there are almost no recombination losses at low photocurrent. As shown in Fig. 2, lower starting photocurrents of saturation, as compared with [21, 22], were obtained at all wavelengths, which are due to higher series resistance of the used n-type Si PDs.

3.2. Spectral linearity characteristics with reverse bias voltage

Figure 3 shows the experimentally measured nonlinearity results at the selected wavelengths at reverse-bias voltage of 10 V. Assuming that the linearity factor, LF(0), at a generated photocurrent of 64 nA was equal to unity, the nonlinearities for each

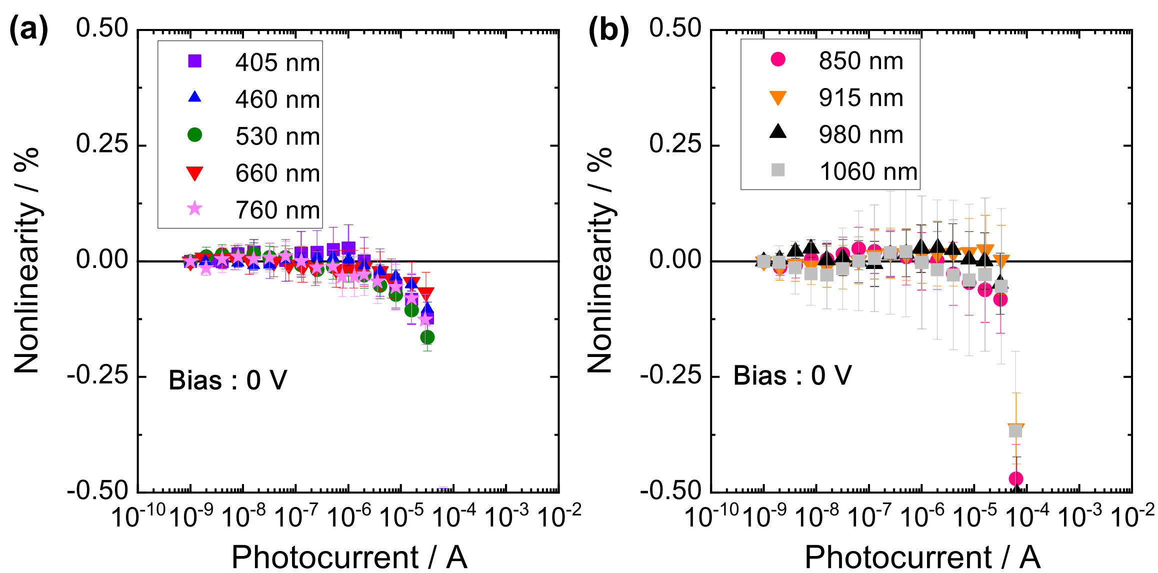

Figure 2. Spectral nonlinearities measured under zero-bias at the wavelengths of 405 nm, 460 nm, 530 nm, 660 nm, and 760 nm (a) and at the wavelengths of 850 nm, 915 nm, 980 nm, and 1060 nm (b). All experimental data are normalized at a photocurrent of 1 nA.

photocurrent were also derived with Eqs. (4) and (5). The solid horizontal lines in Fig. 3 also represent the linear response.

As shown in Fig. 3, the absolute values of the derived nonlinearity of the PQED were less than 0.1 % at the photocurrent from 100 nA to 500 μA at the reverse-bias voltage of 10 V except for the nonlinearity result at 1060 nm. The PQED shows linear response in the photocurrent range from 100 nA to 500 μA except for the nonlinearity result at 1060 nm. This is the first time that the spectral linearity in visible to near-infrared region under the reverse-bias voltage conditions has been confirmed for the PQED based on n-type PDs. Conversely, other n-type Si PDs show supralinear behavior in the near-infrared range under reverse bias conditions [21]. The comparison results with other n-type Si PD under bias conditions revealed that the PQED had no recombination losses that causes supralinearity up to wavelength of 980 nm. The responsivities started to decrease for photocurrents larger than 1 mA at the wavelength from 405 nm to 980 nm, due to the saturation of the PQED. Comparing with the nonlinearity results under zero-bias condition, the starting photocurrents of saturation were increased to over 1 mA by applying the reverse-bias voltage of 10 V because the saturation photocurrent value, I_{sat}, can be derived as a function of the reverse bias voltage as following equation,

$$I_{\mathrm{sat}} = \frac{V_{\mathrm{bi}} + V}{R_{\mathrm{s}} + R_{\mathrm{L}}}, \tag{6}$$

where V_{bi} is the built-in potential, V is the reverse-bias voltage, R_{s} is the series resistance, and R_{L} is the load resistance. A similar tendency was previously reported with an

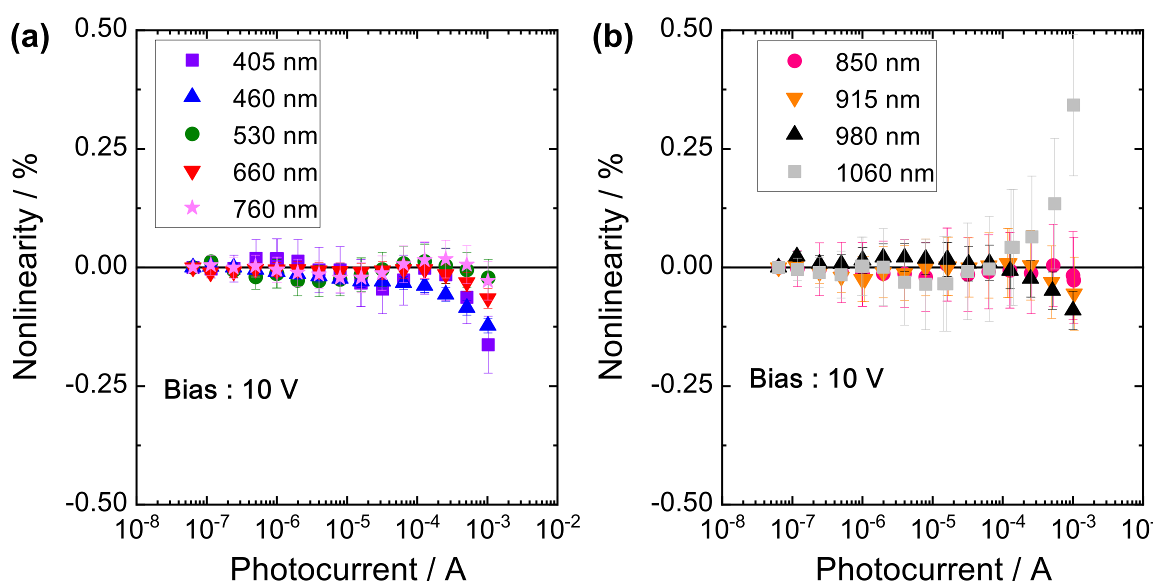

Figure 3. Spectral nonlinearities measured with reverse bias of 10 V at the wavelengths of 405 nm, 460 nm, 530 nm, 660 nm, and 760 nm (a) and at the wavelengths of 850 nm, 915 nm, 980 nm, and 1060 nm (b). All experimental data are normalized at a photocurrent of 64 nA.

inverse-layer-type Si PD [30]. Comparing our results with previous linearity results at 488 nm at the reverse-bias voltage of 10 V [12], these spectral linearity results up to wavelength of 980 nm were similar in terms of linear response and starting photocurrent of the saturation. The spectral linearity results obtained in the visible to near-infrared range using the flux addition method are more detailed and help us to perform more accurate measurement with the PQED as well as provide useful information for modelling the charge-carrier loss mechanisms of the PQED.

On the other hand, as shown in Fig. 3 (b), supralinear behavior of the PQED was clearly observed at 1060 nm under the reverse-bias voltage of 10 V. Its value sharply increased at the photocurrent from 100 μA, and maximum value reached 0.34 % at the photocurrent of 1 mA. To the best of our knowledge, this is first time of such supralinearity behavior of the PQED has been reported. The responsivity for 1060 nm also decreased at the photocurrent over 1 mA, due to saturation. This result indicates that the supralinearity up to 0.34 % occurred because the saturation photocurrent at 1060 nm shifted over 1 mA by applying the reverse-bias voltage of 10 V. This result is also similar to the report with an inverse-layer-type Si PD [30].

The reason why the PQED shows supralinear behavior at 1060 nm can be explained as follows. Although the absorption length of Si up to 980 nm is less than 104 μm, it reaches 901 μm at 1060 nm [31]. It is longer than the PD thickness of the used PQED, 500 μm. Firstly, the incident light reaches the back electrode made of aluminum while being absorbed in the Si bulk, and a part of the light is reflected by this electrode. As a result, Shockley-Read Hall recombination loss would occur in the Si bulk as the absorption length of Si at 1060 nm is longer than the used PD thickness even though the recombination life time is as long as 28 ms. Secondly, the n-type Si PD generally consists of the heavy doped n^+-type layer next to the n-type layer at the back electrode, which functions as a potential barrier to suppress the back surface recombination [32]. However, such recombination could occur near the back electrode of the PQED since the absorption length of Si at 1060 nm is longer than the used PD thickness. The use of electrode material that generates no recombination at the back electrode and of thicker Si PD help us to suppress the back surface recombination.

4. Conclusion

Spectral nonlinearity of PQED was investigated in the wavelength range from 405 nm to 1060 nm under zero-bias and reverse-bias voltage conditions. In zero-bias condition, the linear behavior was obtained at the photocurrent of 1 nA to 10 μA, and the saturation occurred at the photocurrent over 10 μA for all wavelengths. In the reverse-bias voltage of 10 V, the linear behavior was observed at the photocurrent 64 nA to 1 mA except for 1060 nm. In comparison with the results under the zero-bias condition, the saturation photocurrent was shifted over 1 mA. We conclude that the PQED shows linear response in the photocurrent range of 1 nA to 1 mA in the wavelength range of 405 nm to 980 nm by applying the appropriate bias voltage to it. It is also speculated that the PQED has linear response below 1 nA. In contrast, the response of the PQED at 1060 nm sharply increased at the photocurrent from 100 μA, and maximum supralinearity value reached up to 0.34 % at the photocurrent of 1 mA. We considered that the reasons for this supralinear behavior were the back surface recombination and the longer absorption length for 1060 nm in Si. The spectral linearity results are expected to help us to perform more accurate measurement with the PQED in the fields of radiometry and photometry, and to provide fruitful information for modelling the charge-carrier loss mechanisms of the PD.

5. Acknowledgements

The authors acknowledge that the research leading to these results has received funding from the European Metrology Research Programme (EMRP) project SIB57 New Primary Standards and Traceability for Radiometry and from the Academy of Finland Flagship Programme, Photonics Research and Innovation (PREIN), decision number: 320167.

References

[1] Martin J E, Fox N P and Key P J 1985 A cryogenic radiometer for absolute radiometric measurements *Metrologia* **21** 147–155

[2] Varpula T, Seppa H and Saari J M 1989 Optical power calibrator based on a stabilized green He-Ne laser and a cryogenic absolute radiometer *IEEE Transactions on Instrumentation and Measurement* **38** 558–564

[3] Zalewski E F and Geist J 1980 Silicon photodiode absolute spectral response self-calibration *Appl. Opt.* **19** 1214–1216

[4] Geist J, Zalewski E F and Schaefer A R 1980 Spectral response self-calibration and interpolation of silicon photodiodes *Appl. Opt.* **19** 3795–3799

[5] Geist J, Liang E and Schaefer A R 1981 Complete collection of minority carriers from the inversion layer in induced junction diodes complete collection of minority carriers from the inversion layer in induced junction diodes *J. Appl. Phys.* **52** 4879–4881

[6] Zalewski E F and Duda C R 1983 Silicon photodiode device with 100% external quantum efficiency *Appl. Opt.* **22** 2867–2873

[7] Gran J and Sudbø A S 2004 Absolute calibration of silicon photodiodes by purely relative measurements *Metrologia* **41** 204–212

[8] Gran J and Tang C K 2017 Validation that Hamamatsu 1337 trap detectors are independently predictable when using a hybrid self-calibration method *Proceedings of NEWRAD 2017* 168–169

[9] Sildoja M, Manoocheri F, Merimaa M, Ikonen E, Müller I, Werner L, Gran J, Kübarsepp T, Smid M and Rastello M L 2013 Predictable quantum efficient detector: I. photodiodes and predicted responsivity *Metrologia* **50** 385–394

[10] Müller I, Johannsen U, Linke U, Socaciu-Siebert L, Smid M, Porrovecchio G, Sildoja M, Manoocheri F, Ikonen E, Gran J, Kübarsepp T, Brida G and Werner L 2013 Predictable quantum efficient detector: II. characterization and confirmed responsivity *Metrologia* **50** 395–401

[11] Dönsberg T, Sildoja M, Manoocheri F, Merimaa M, Petroff L and Ikonen E 2014 A primary standard of optical power based on induced-junction silicon photodiodes operated at room temperature *Metrologia* **51** 197–202

[12] Dönsberg T, Manoocheri F, Sildoja M, Juntunen M, Savin H, Tuovinen E, Ronkainen H, Prunnila M, Merimaa M, Tang C K, Gran J, Müller I, Werner L, Rougié B, Pons A, Smîd M, Gál P, Lolli

L, Brida G, Rastello M L and Ikonen E 2017 Predictable quantum efficient detector based on n -type silicon photodiodes *Metrologia* **54** 821–836

[13] *SI Brochure (2019) Mise en pratique for the definition of the candela and associated derived units for photometric and radiometric quantities in the SI* (BIPM)

[14] Lehman J 1997 Pyroelectric trap detector for spectral responsivity measurements *Appl. Opt.* **36** 9117–9118

[15] Sildoja M, Manoocheri F and Ikonen E 2009 Reflectance calculations for a predictable quantum efficient detector *Metrologia* **46** S151–S154

[16] Dönsberg T, Pulli T, Poikonen T, Baumgartner H, Vaskuri A, Sildoja M, Manoocheri F, Kärhä P and Ikonen E 2014 New source and detector technology for the realization of photometric units *Metrologia* **51** S276–S281

[17] Pulli T, Dönsberg T, Poikonen T, Manoocheri F, Kärhä P and Ikonen E 2015 Advantages of white LED lamps and new detector technology in photometry *Light. Sci. Appl.* **4** e332–1–7

[18] Dönsberg T, Mäntynen H and Ikonen E 2016 Optical aperture area determination for accurate illuminance and luminous efficacy measurements of LED lamps *Optical Review* **23** 510–521

[19] Porrasmaa S, Dönsberg T, Manoocheri F and Ikonen E 2020 Predictable quantum efficient detector for low optical flux measurements *Optical Review* **27** 190–194

[20] Haapalinna A, Kübarsepp T, Kärhä P and Ikonen E 1999 Measurement of the absolute linearity of photodetectors with a diode laser *Meas. Sci. Technol.* **10** 1075–1078

[21] Tanabe M, Amemiya K, Numata T and Fukuda D 2015 Spectral supralinearity prediction of silicon photodiodes in the near-infrared range *Appl. Opt.* **54** 10705–10710

[22] Tanabe M, Amemiya K, Numata T and Fukuda D 2016 Spectral supralinearity of silicon photodiodes in visible light due to surface recombination *Appl. Opt.* **55** 3084–3089

[23] Salffner K, Dönsberg T, Porrovecchio G, Smid M, Nield K and Nevas S 2018 Characterization of a room temperature predictable quantum efficient detector for applications in radiometry and photometry *Metrologia* **55** 654–661

[24] Tang C K, Gran J, Müller I, Linke U and Werner L 2015 Measured and 3d modelled quantum efficiency of an oxide-charge induced junction photodiode at room temperature *2015 International Conference on Numerical Simulation of Optoelectronic Devices (NUSOD)* pp 177–178 ISSN 2158-3242

[25] Arnold A S, Wilson J S and Boshier M G 1998 A simple extended-cavity diode laser *Review of Scientific Instruments* **69** 1236–1239

[26] Hawthorn C J, Weber K P and Scholten R E 2001 Littrow configuration tunable external cavity diode laser with fixed direction output beam *Review of Scientific Instruments* **72** 4477–4479

[27] Hall R N 1952 Electron-hole recombination in germanium *Phys. Rev.* **87** 387

[28] Shockley W and W T Read J 1952 Statistics of the recombinations of holes and electrons *Phys. Rev.* **87** 835–842

[29] Schroder D K 2006 *Semiconductor Material and Device Characterization, 3rd Edition* (Wiley-IEEE Press)

[30] Tanabe M, Zama T and Shitomi H 2017 Experimental validation of nonlinearity suppression for an inverse-layer-type silicon photodiode and its prediction based on theoretical modeling *Appl. Opt.* **56** 5804–5810

[31] Green M A 2008 Self-consistent optical parameters of intrinsic silicon at 300 K including temperature coefficients *Solar Energy Materials and Solar Cells* **92** 1305–1310

[32] Fossum J G 1977 Physical operation of back-surface-field silicon solar cells *IEEE Transactions on Electron Devices* **24** 322–325